Numerical investigation of vertical-axis tidal turbines with sinusoidal pitching blades

Numerical Investigation of Vertical-Axis Tidal Turbines with Sinusoidal Pitching Blades

Bing Chen[1*], Shaoshuai Su[1], Ignazio Maria Viola[2], Clive A Greated[3]

[1]School of Ocean Science and Technology, Dalian University of Technology, China

chenbing@dlut.edu.cn

[2] School of Engineering, Institute for Energy Systems, The University of Edinburgh, Scotland, UK

i.m.viola@ed.ac.uk

[3] School of Physics and Astronomy, The University of Edinburgh, Scotland, UK

c.a.greated@ed.ac.uk

ABSTRACT

In this paper, numerical simulations are conducted to compare the performances of a fixed-blade vertical-axis turbine (VAT), and a variable pitch VAT whose blades are forced to do sinusoidal pitching. The numerical model is based on the Navier-Stokes equations and shear stress transport (SST) k-ω turbulence model. At first, the output characteristics of fixed-blade turbines and variable pitch turbines with different amplitude of pitching, including power coefficient, torque coefficient and ripple factors, are compared. Then the hydrodynamic torques, tangential and normal forces on a blade are compared as well. The comparison reveals that sinusoidal pitching of the blades greatly improves the performance of the turbine. With an appropriate amplitude of pitching, not only the power efficiency increases, but the fluctuation in power output, rotation speed and torque output are suppressed as well. Results also show that the hydrodynamics forces on a blade of a variable pitch turbine are lower than those of the fixed-blade turbine.

Keywords: Vertical-axis turbine; Variable pitch; Numerical simulation; Power coefficient; Hydrodynamic forces

1. Introduction

So far it seems that horizontal-axis wind turbines have won the competition with vertical-axis wind turbines in the large-scale wind power industry. However, in the field of tidal stream energy exploitation, it is still too soon to make a conclusion about their competition. Some advantages of VAT's that seem not so critical for wind turbines become more significant for tidal turbines. These advantages include structural simplicity, adaption to flow of arbitrary direction, the ability to transmit torque directly above the water surface, *etc*. The latter perhaps is the most significant one because it greatly reduces maintenance costs since no underwater working is needed any more. A straight-blade vertical-axis turbine, often referred to as H-Darrieus turbine, is one of the most popular vertical-axis turbines due to its easy manufactured blade and good performance. These turbines have been the objectives of several studies such as, for instance, the work of Gosselin (2015) and Gosselin *et al* (2016), in which parametric study on the effects of rotor solidity, blade thickness, fixed pitch angle, and blade aspect ratio *etc.* to the performance of the turbine were carried out. These turbines achieve maximum power efficiency at an optimal tip-speed ratio (TSR) and solidity for a given flow condition; higher solidity reduces peak efficiency and lowers the optimal TSR, but helps to improve the poor self-starting performance to some extent; the angle of attack of blade varies periodically due to its motion on a circular path and introduces vibrations into the shaft torque and rotation; using more blades helps to reduce torque and rotation fluctuations.

The disadvantages of Darrieus turbines compared to the horizontal-axis turbine are, for instance, the relative lower overall efficiency, higher fluctuation in torque and rotational speed, inability to self-start reliably, a narrower band of tip-speed ratios to achieve good efficiency, and that the blades experience large

* Tel: 86-427-2631663
Fax: 86-427-2631888
Email: chenbing@dlut.edu.cn

angle of attack variation. Some efforts have been made to overcome the disadvantages of conventional H-Darrieus turbines. For example, the turbine could be incorporated with a duct to increase power output and reduce the torque fluctuation substantially. However, the cost of building a duct device is much greater than that of the turbine itself, due to its large size and hence the large hydrodynamic load that it experiences. Unless serving also as support structure, building a duct device only for the purpose of performance improvement is not economically feasible. Gorlov (1995, 1998) developed a novel turbine which uses helical twisted blades. By distributing the blade sections over a large fraction of the circumference of its circular path, the Gorlov helical turbine is reported to have greater efficiency, no torque fluctuation, and improved self-start performance. However, to manufacture a helical twisted blade is more complicated and, hence, more expensive than a straight blade. Furthermore, the angle of attack of fixed helical blades cannot be adjusted to avoid stall.

It has been found that the performance of a H-Darrieus turbine can be greatly improved, especially if the turbine operates at lower tip-speed ratio, by allowing the blades to pitch cyclically, so as to avoid stall and maintain favorable angles of attack as long as possible. The optimal pitch angle is a function of both the azimuthal position and the tip-speed ratio of the blade. The mechanisms for achieving pitch variation fall into two categories. One is active or forced pitching, which means that the blade is forced to pitch according to some predetermined schedule. Another is passive, or so-called self-acting pitching, which means that the blade is free to pitch under the interaction between the fluid dynamic force, the inertial force, and stabilizer moments. Passive variable pitch requires many fewer mechanical parts.

According to Kirke and Lazauskas (1991), both active and passive variable pitch concepts for vertical-axis wind turbines were already known in the late 1970s, but no performance data for actual prototypes had been published until early 1990s. Since then a lot of works on variable pitch wind turbines have been reported. Kirke and Lazauskas (1991) developed the earliest mathematical model based on an extended double-multiple streamtube (DMS) approach to predict the performance of passive pitch systems. Similar mathematical models have been adopted in later investigations such as, for instance, those of Lazauskas (1992), Staelens *et al.* (2003), Paraschivoiu *et al.* (2009), and Chougule *et al.* (2014). More complex models have also been introduced to get more accurate prediction of flow behavior around blades, *e.g.* the vortex model in Erickson *et al.* (2011), the RANS models in Miau *et al.* (2012) and Gosselin (2015) *etc*. Many researchers conducted wind tunnel experiments to confirm their predictions with mathematical models as, for instance, Kirke and Lazauskas (1993), Erickson *et al.* (2011). Most recently, Kirke and Paillard (2017) use both DMS model and 2-D RANS model to predict the performance of a vertical axis wind turbine in both fixed and variable pitch modes, and compared with field test data. They revealed that variable pitch enables to overcome two major disadvantages of normal fixed pitch vertical axis wind turbines, *i.e.* self-starting and overspeed control.

The strategies of variable pitch have been the objective of many studies. For active pitch control, pitch variation allow the blades to operate always at the optimal angle of attack for every azimuth position, but this control imposes high complexity on the system. Two simpler options to decrease the occurrence of dynamic stall are: either to maintain the blades' angle of attack on a predetermined angle as long as possible, or to make the blades' pitch angle following a sinusoidal variation. Lazauskas (1992) analyze the performance of vertical-axis wind turbines with three variable pitch mechanisms, a sinusoidal forced pitch variation, and two kinds of self-acting stabilized pitch controls. He reported that all the pitch control systems examined can be configured to produce a better starting torque, a broader operating range and greater efficiency than a fixed pitch turbine. Staelens *et al.* (2003) presented three strategies for actively varying the pitch angle. The first two require accurate control to keep the angle of attack under the stall angle, while the last one aims to adjust the pitch angle following a simple sinusoidal function. The authors conclude that although the power output obtained by using sinusoidal pitching is less than the other two strategies, it doesn't present any physical and mechanical difficulty and thus it is most practically feasible. As a further develop to Staelens *et al.* (2003), Paraschivoiu *et al.* (2009) use a genetic algorithm optimizer to find the

optimal pitch variation which relating the blades' pitch to the local flow conditions along their circular path. The results show that a pitch variation is optimal only for a given TSR. Using a strategy to ensure an almost constant angle of attack during the whole cycle of blade motion, Gosselin (2015) report that the overall efficiency of a Darrieus turbine operating at tip-speed ratio 3.4 could exceed by 50% that predicted by a two-dimensional RANS model.

The concept of variable pitch blades is logically transferred from wind turbines to tidal turbines. Gosselin (2015) concludes that variable pitch is not particularly efficient for wind turbines that have low solidities and operate at high tip-speed ratios. For a hydrokinetic turbine operating at lower tip-speed ratios, the gain from variable blade pitch could be much larger. While the typical optimal tip-speed ratio for vertical-axis wind turbines usually ranges from 4 to 6, Salter (2005) suggests that the tip-speed ratio of vertical-axis tidal turbines should be less than 2.5 to avoid serious cavitation effect. Schönborn and Chantzidakis (2007) suggest a relative velocity between the blades and the water below 8.45 m/s to avoid cavitation for a symmetric NACA0018 blade. The lower tip-speed ratio of tidal turbines makes variable pitch particularly attractive. Due to their mechanical simplicity, passive variable pitch turbines have been the first to be tested at sea. A 50kW Italian Kobold vertical-axis turbine with self-acting variable pitch straight blades has been installed at sea in 2001. Coiro *et al.* (2005) analyze the performance of the Kobold turbine with a DMS model. The theoretical predictions are in good agreement with the results from laboratory tests and sea trails. Hantoro *et al.* (2011) carried out experimental investigations on the performance of a passive variable pitch turbine in a towing tank and confirmed the enhanced ability to start rotating at intermediate TSRs and the lowered occurrence of stall. Lazauskas and Kirke (2012) used a memetic algorithm to optimize pitch parameters for passive pitch control systems. A DMS type model predicts that the peak efficiency is about 50% higher than an equivalent fixed pitch turbine. Self-starting ability and vibration performance are greatly improved as well.

Along with the progress of electromechanical equipment and automatic control technology, the cost and reliability of active pitch control are set to improve and achieve an acceptable level. Active variable pitch can always optimize the pitch angle of blades according to flow condition, while the parameters of a passive variable pitch can only be changed with difficulty once they have been set. Therefore, theoretically the former should let the turbine achieve better performance than the latter. Pitch actuation for active variable pitch vertical-axis turbine consumes significant power. Salter and Taylor (2007) suggest that if the pivot of the blade pitching is properly placed ahead of the centre of pressure, then blade pitch movement will generate power rather than consuming it. This produced power partially compensates for the consumed power, so that the mean power needed to actuate the blades during a turbine's revolution is minimal. Paillard *et al.* (2013) incorporate a dynamic stall model into a streamtube model to investigate the performance of a Darrieus turbine with active pitch variation. A maximum increase on the power coefficient of 53% is reported for a sinusoidal pitch variation, when the power consumption required for blade pitching is lower than 1%. A general discussion on the performance of variable pitch hydrokinetic turbines can be found in Kirke and Lazauskas (2008, 2011).

Beside those focused on pitch control strategy, there are also studies on mechanic devices that actuating the blades such as, for instance, Grylls *et al.* (1978) and Vandenberghe and Dick (1986) for wind turbines, and a novel hydraulic control mechanism in Schönborn and Chantzidakis (2007) for tidal turbine in marine environment.

In this paper, numerical simulations based on a two-dimensional incompressible viscous flow model are carried out to further investigate the performances of a fixed-blade turbine and an active variable pitch turbine whose blades are forced to do sinusoidal pitching are compared. The output characteristics of fixed and variable pitch turbines with different amplitude of pitching are compared; the variations of power coefficient, torque coefficient, ripple factors, hydrodynamic torques, tangential and normal forces on a blade are discussed. To the knowledge of the authors, the rotational speed is always set to a series of constant values in existed numerical investigations on vertical-axis turbines. Differently from existed

studies, in this paper the rotational speed is obtained by solving the motion equation at every time step, so that the influence of variable pitch on the rotational speed could be assessed as well. The effect of variable pitch to the hydrodynamic forces on the blades is also hardly found in existed studies, whilst it is a focal point of this paper, too.

2 Numerical Model

2.1 Flow Model

A commercial computational fluid dynamic (CFD) software, Ansys Fluent, is used to solve the Reynolds-Averaged Navier-Stokes (RANS) equations with a cell-based finite volume method. The onset tidal stream is turbulent, as well as the flow across the turbine rotor. The effect of the turbulence is modelled with a κ-ω SST turbulence model across the entire domain. Therefore, the boundary layer on the blades is also modelled as turbulent. It is assumed, in fact, that biofouling would trigger laminar to turbulent transition at a location in the boundary layer very close to the leading edge; even if the blade's Reynolds number based on the blade chord and the relative flow velocity for a tip speed ratio of 1.5 is 2.25×10^5. This choice of the turbulence model is also consistent with that of other authors who tested VAT's at similar Reynolds numbers (for instance, Marsh *et al*., 2015).

Li and Calisal (2010) and Marsh *et al.* (2015) have used three-dimensional models to simulate vertical-axis turbines. They reported that the arm has a significant effect on the turbine power output prediction. On the other hand, as pointed out by Li and Calisal (2010), the computational time of three-dimensional models capable of accounting for this effect, is more than thirty times that of the present two-dimensional model. Therefore, in this paper we neglect this important effect to enable a wide parameter study. The focus of this paper is, therefore, the difference between the fixed and the variable pitch, while the effects of arms as well as the finite length of the blades are ignored.

2.2 Rotor Dynamics

The hydrodynamic torque on the rotor, Q_H, is obtained by adding the torques of all the three blades. Other than the hydrodynamic torque, there is a resistant torque due to several sources, including the electromagnetic force between the stator and the translator of the generator, the friction at the bearings, the seal rings, between gear teeth, *etc*. In this paper, all resistant torques are accounted for by the load torque Q_L. The equation of the rotation of the rotor is

$$J_z \frac{d\omega}{dt} = Q_H(t) + Q_L(t), \tag{1}$$

where J_z is the rotational inertia of the rotor from its vertical axis, ω is the angular velocity of the rotor that is solved at every time step, and t is the time. To a first approximation, the load torque is assumed to be proportional to the rotational speed of the shaft.

$$Q_L(t) = -b\omega(t), \tag{2}$$

where the load coefficient b is a positive constant which reflects the features of the electricity generator and the electrical load in the circuit or the grid. It should be noted that the assumption of a linear relation between load torque and rotational speed is not universally valid, since the load torque depends on load characteristics including electrical architecture and the friction in mechanical system.

Different strategies for active blade-pitching have been proposed. For example, Lazauskas (1992) forced the pitch angle of the blade to vary sinusoidally from an initial blade offset angle. Salter (2005) proposed an asymmetric curve of pitch angle variation and indicated that the maximum pitch change occurs at

azimuthal angle θ (reference to Fig. 1) later than 90° and earlier than 270°. Hwang *et al.* (2009) applied a genetic algorithm to determine the optimal pitch angle curves for different tip-speed ratios. An optimal pitch angle variation may give better performance to the turbine but may also increase the machinery complexity. In practice, engineering reliability follows from mechanical simplicity, even though performance can be traded off to some degree. In this paper, blades are forced to pitch following a simple sinusoidal variation. At the azimuthal angles $\theta = 0°$ and 180°, the pitch angle is set to zero, thus the sinusoidal variation of the pitch angle is

$$\varphi = \varphi_{amp} \sin\theta, \tag{3}$$

where φ is the instantaneous pitch angle of the blade and φ_{amp} is the amplitude of the pitch variation. The pitch angle is positive when the leading edge of the blade points outward to the rotor. The variation of the pitch angle of the blades at different azimuthal position is presented in Fig.1, where both the size and the pitch angle of the blades are exaggerated to give a clear illustration. In the figure, F_{Tb} and F_{Nb} are the tangential and normal hydrodynamic forces acting on the blade, and l_T and l_N are the arms of these forces. Note that the tangential force is defined positive from the trailing edge to the leading edge of the blade, and thus it is not tangential to the circular orbit of blades. For fixed-blade turbines, where the pitch angle is always zero, the normal force on the blades provides a negligible contribution to the driving torque if the offset between the pivot of a blade and its center of pressure is neglected. However, in the case of variable pitch turbines, both tangential and normal forces contribute to the driving torque, as clearly displayed in the figure.

According to Eq. (3), the amplitude of pitch variation φ_{amp} is the only parameter that can be adjusted, and it is expected to have significant influence on the performance of the turbine. In this paper, five values of the parameter φ_{amp} are tested (2.5°, 5°, 10°, 12°, and 15°) to investigate its influence on the performance of the turbine.

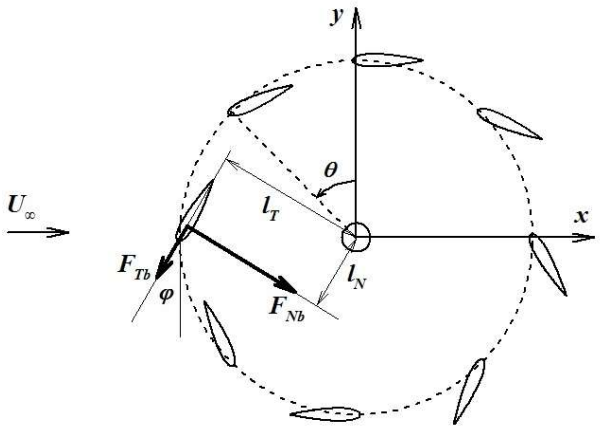

Fig.1: Schematic drawing of different positions of a blade section during a period of revolution.

2.3 Geometry, Computational Domain and Grid

The parameters of the H-Darrieus turbine used in this study are given in Table 1. The pivots of the blades are located at 1/10th of the chord from the leading edge.

The layout of the computation domain is shown in Fig. 2 (not to scale). The length of the computation domain is 266 chord lengths (C); the distance from the inflow boundary to the centre of the rotor is 66C; the width of the computation domain is 106C. This size of the computatioanl domain is comparable to that of Kirke and Paillard (2017), who used a domain size of 10×30 D (67C×*200*), where D is the diameter of the rotor.

Table 1: Specifications of the tested vertical-axis turbine

Diameter of rotor, D (m)	1.0
Radius of rotor, R (m)	0.5
Diameter of shaft, D_0 (m)	0.04
Height of the blade, H (m)	1.0
Swept area of the rotor, $A=HD$ (m^2)	1.0
Number of blades, N	3
Blade airfoil	NACA0018
Blade chord, C (m)	0.15
Solidity, $\sigma = NC/R$	0.9
Rotational inertia, J_z (kg m^2)	1.5

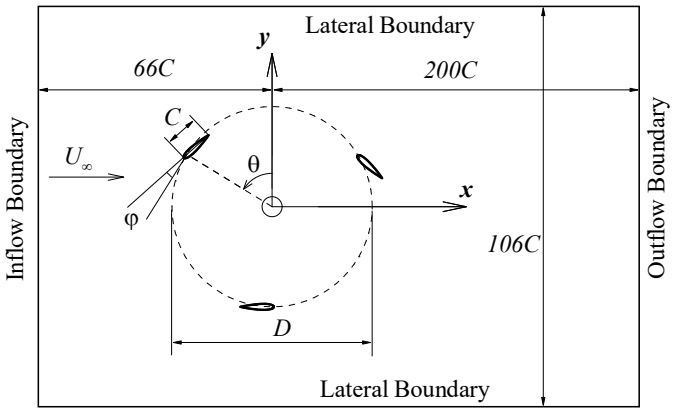

Fig. 2: Schematic layout of the computational domain (not to scale).

The grid around the rotor moves following the rotation of the rotor, and the grid around the blades rotates when the blades are pitching around their pivots. To cope with these complex motions the grid is divided into several zones as shown in Fig. 3 (a), including: the blade zones around each blade; a rotor zone around the rotor and containing all blade zones; an outer zone covering the whole computational domain and containing the rotor zone. The grids in adjacent zones slide along the interfaces. The blade zones are further divided into sub-zones according to geometric features. Each zone or sub-zone is mapped by a structural mesh with quadrilateral cells, as shown in Fig. 3 (b).

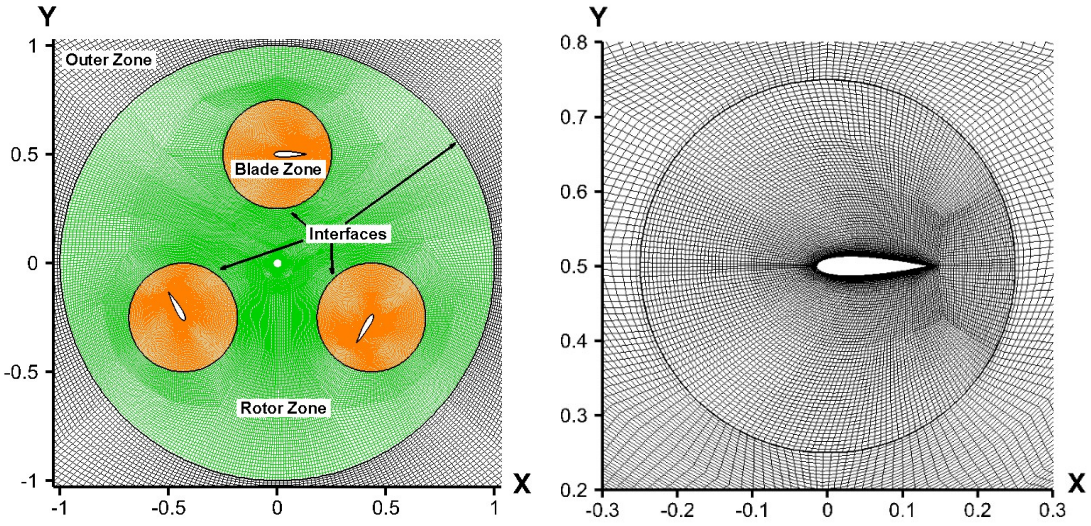

(a) Grid zones. (b) Detailed grid around the blade.

Fig. 3: Grid and sliding interfaces.

2.4 Boundary Conditions

A uniform velocity is prescribed at the inlet boundary. The fluid is accelerated from zero at rate a=1.0 m/s^2 until the steady speed U_∞=1.0 m/s is reached. On the outflow boundary, a zero reference pressure is set. A 'symmetry' boundary condition is used on the lateral boundaries, while a no-slip 'Wall' condition is applied on all the solid surfaces of the blades and on the shaft of the rotor. These boundary conditions for velocity and pressure are summarized below:

$$\begin{cases} \vec{u} = (\min\{at, U_\infty\}, 0), \text{ on inlet boundary,} \\ p = 0, \text{ on outflow boundary,} \\ \vec{u} \cdot \hat{n} = 0, \ \dfrac{\partial \vec{u}}{\partial \mathrm{n}} = 0, \text{ on lateral boundaries,} \\ \vec{u} = \vec{\omega} \times (\vec{x}_b - \vec{x}_c), \text{ on surface of the shaft,} \\ \vec{u} = \vec{\omega} \times (\vec{x}_b - \vec{x}_c) + \vec{\omega}_{pitching} \times (\vec{x}_b - \vec{x}_{pivot}), \text{ on surfaces of the blades,} \end{cases} \tag{4}$$

where $\hat{n}$ are normal unit vectors to the boundary surfaces; $\vec{x}_b$, $\vec{x}_c$ and $\vec{x}_{pivot}$ are the coordinate vectors of points on the solid surfaces, the center of the rotor's axis, and the pivots of the blades, respectively; $\vec{\omega}$ and $\vec{\omega}_{pitching}$ are the vector of rotational speeds of the rotor and the blades' pitching motion, respectively. Both $\vec{\omega}$ and θ are obtained by integrating Eq. (1), then $\omega_{pitching}$ is derived from a rearward differences based on pitch angles predetermined by Eq. (3) at present and previous time steps. These calculations are implemented through User Defined Functions (UDF).

The turbulent kinetic energy k and the specific dissipation rate ω at the inlet are such that the turbulent intensity I (defined as the ratio of the root-mean-square of the velocity fluctuations u', to the mean flow velocity $\bar{u}$) is

$$I \equiv \frac{u'}{\bar{u}} = 5\%, \tag{5}$$

and the turbulent viscosity ratio (defined as the ratio of turbulent viscosity μ_t to the molecular viscosity μ) is

$$\frac{\mu_t}{\mu} = 10, \tag{6}$$

At the wall boundaries, the roughness height is zero, which corresponds to smooth walls.

2.5 Data Analysis

As explained above, the rotational speed and the azimuthal angle can be obtained by integrating the motion equation of the rotation of the rotor with respect to time t:

$$\omega(t) = \int_0^t \left(\frac{d\omega}{dt} \right) dt, \quad \theta(t) = \int_0^t \omega dt, \tag{7}$$

The instantaneous torque on the shaft is opposite to the load torque acting on the shaft:

$$Q_o(t) = -Q_L(t) = b\,\omega(t), \tag{8}$$

The instantaneous power output by the turbine is the product of the torque on the shaft and the rotational speed:

$$P(t) = Q_o(t)\omega(t) = b[\omega(t)]^2, \tag{9}$$

The power coefficient C_p is defined as the ratio between the time-averaged power output and the power of the tidal flow passing the swept area of the rotor:

$$C_p = \frac{\overline{P}}{\frac{1}{2}\rho U_\infty^3 A} = \frac{b\overline{\omega^2}}{\frac{1}{2}\rho U_\infty^3 DH}, \tag{10}$$

in which ρ is the water density. C_p represents the fraction of the kinetic energy of the tidal current that is extracted by the turbine and is therefore a measure of the tidal current energy conversion efficiency.

For convenience of comparison, the results are presented in non-dimensional form. The non-dimensional instantaneous power output is defined as

$$C_p' = \frac{P(t)}{\frac{1}{2}\rho U_\infty^3 DH}, \tag{11}$$

Compared to Eq. (10), the power coefficient could be regarded as the non-dimensional time-averaged power output. The non-dimensional torque output at the shaft is the torque coefficient C_q. Its instantaneous and time-averaged values are defined as:

$$C_q = \frac{Q_L}{\frac{1}{2}\rho U_\infty^2 DHR} = \frac{b\omega}{\frac{1}{2}\rho U_\infty^2 DHR}, \qquad \overline{C_q} = \frac{b\overline{\omega}}{\frac{1}{2}\rho U_\infty^2 DHR}, \tag{12}$$

The instantaneous rotational speed of the rotor is non-dimensionalized as λ'. The non-dimensionalized time-averaged rotational speed is named tip-speed ratio λ :

$$\lambda' = \frac{\omega R}{U_\infty}, \qquad \lambda = \frac{\overline{\omega} R}{U_\infty}, \tag{13}$$

All the overall output of the turbine, including power output, rotational speed, and torque coefficient, exhibit periodic fluctuations in running. These fluctuations are a main disadvantage of a VAT, since these wear the mechanical transmission system and cause unfavorable effect on the electric circuit/grid. Therefore, the characteristics of these fluctuations are worthy of study. Ripple factors of these variables are defined as

$$R_f = \frac{\bar{f}_{\max} - \bar{f}_{\min}}{\bar{f}}, \tag{14}$$

in which f represents power output, or rotational speed, or torque coefficient; $\bar{f}_{max}$, $\bar{f}_{min}$ and $\bar{f}$ are the maximum, minimum, and mean of the phase-averaged values of these variables, respectively.

At the beginning of the simulations, the onset flow speed is increased gradually. The results presented hereafter are referred to the data recorded after the transient start, when all quantities vary periodically. Mean and statistics are computed over 10 to 20 cycles, depending on the tip-speed ratios.

2.6 Grid and Time Step Uncertainty Quantification

The uncertainty due to the grid and time resolution in the computation of the tip-speed ratio, power coefficient and ripple factors of rotational speed is assessed. The uncertainty is computed within a 95%

confidence level using the methodology proposed by Viola *et al.* (2013). The time series of non-dimensional rotational speed and hydrodynamic torque on one blade are shown in Fig. 4 for three grids uniformly refined. Grids with 137554, 219391, and 315714 nodes are referred to as Grid 1, 2, and 3 in the figure, respectively. Grid 2, which has an intermediate resolution, is the reference grid used for this study. In all the simulations, the load coefficient b is set to 5.0 N.m.s and the time step is 0.001 s. For both Grid 2 and 3, y^+ is less than 3 on most part of blades' surface except at the leading edges where it is up to 5. For the coarest grid, Grid 1, y^+ is less than 5 and up to 16 at the leading edge.

The results for the torque coefficient and the non-dimensional power output are similar to those for the non-dimensional rotational speed, and thus are not presented for brevity. Since slightly different rotational speeds are predicted using different grids, this results in phase differences for all variables. For convenience of comparison, the phases of azimuthal angle of three numerical results are forced to align at t=23 s. The differences between results of Grid 2 and Grid 3 are significantly smaller than those between Grid 1 and Grid 2. The coarsest grid (Grid 1), shows a lower trough in the rotational speed curve and hence a phase lag compared to the results of finer grids. Another apparent difference is that the curve of hydrodynamic torque on a blade predicted by the coarsest grid has a sharper secondary peak which does not appear in the predictions of finer grids.

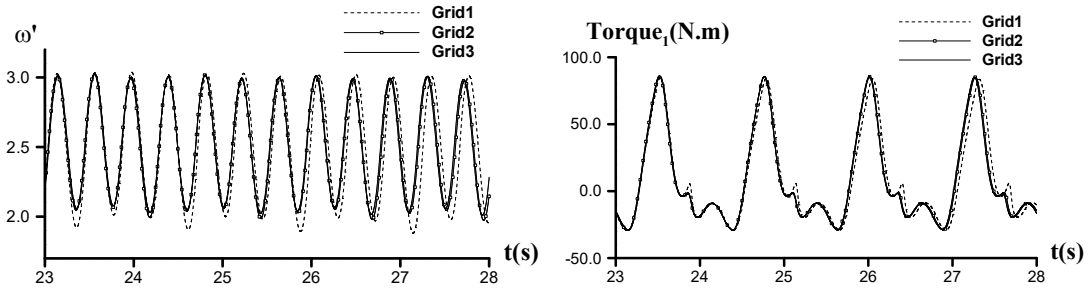

(a) Non-dimensional rotational speed over 5 s. (b) Hydrodynamic torque on a blade over 5 s.

Fig.4 Comparison of numerical results of progressively finer grids.

Table 2: Values of λ, C_p and R_ω computed with different grids and time steps.

	Grid 1	Grid 2	Grid 3	Δt_1	Δt_2	Δt_3	Δt_4	Δt_5
λ	2.473	2.494	2.506	2.477	2.482	2.494	2.516	2.539
C_p	0.251	0.254	0.256	0.251	0.252	0.254	0.258	0.263
R_ω	0.458	0.415	0.402	0.424	0.421	0.415	0.398	0.380

Table 3: Uncertainties at 95% confidence level of λ, C_p and R_ω computed with Grid 2 and Δt_3.

	U_g	U_t	$U_N=(U_g+U_t)^{1/2}$
λ	4%	5%	7%
C_p	6%	10%	11.5%
R_ω	7%	3%	8%

The tip-speed ratio λ, the power coefficients C_p and the ripple factor of the rotational speed R_ω predicted by Grids 1, 2, and 3 are showed in Table 2. The table also includes the values computed with Grid 2 and different time steps: Δt=0.00025 s, 0.0005 s, 0.001 s, 0.002 s and 0.003 s. The uncertainty within a 95% confidence level due to the grid resolution, (U_g) and due to the time resolution (U_t) are shown in Table

3 for λ, C_p and R_ω. The Euclidean norm of the uncertainties due to the grid and time resolutions provides an estimate of the total numerical uncertainty (U_N). These results show that the results presented in the rest of the paper should be considered within an accuracy of $\pm$7%, $\pm$11.5% and $\pm$8% for λ, C_p, and R_ω, respectively.

3. Comparison with Experimental Data

In previous study Chen *et al.* (2017) have compared the power coefficient of a forced rotating turbine computed with the present numerical model with that measured experimentally by Shiono *et al.* (2000). For the sake of completeness, the comparison is presented below with more supplements, such as the grid around the rotor and the results of a few simulations on a hydrodynamic-driven turbine. The airfoil of the blade is NACA63$_3$-018, which is a symmetric foil, but by joining the camber line to the circumference of the rotor, it becomes asymmetric. The variations of power efficiency with respect to tip-speed ratio of a three-blade turbine with solidity (defined as $\sigma = NC/2\pi R$ in Shiono *et al.*, 2000) of 0.366 are used. The grid used is shown in Fig. 5.

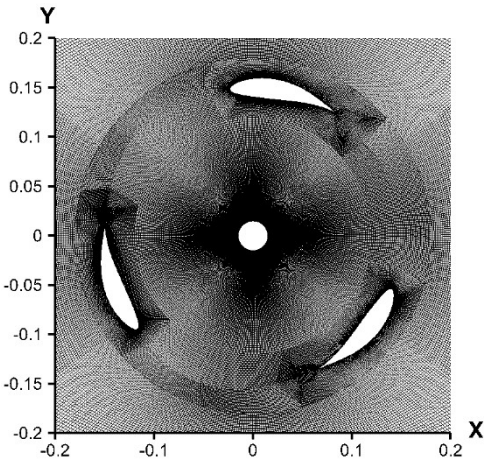

Fig.5 Grid used for model validation.

Both hydrodynamic-driven and forced rotation of the turbine are simulated numerically. In the former case the friction torque on the shaft is adjusted to get different tip-speed ratios. The instantaneous power output and the power coefficient are calculated following Eqs. (9) and (10). In the latter case, constant rotational speeds are assigned to the turbine, and the power output is obtained by multiply the hydrodynamic torques on the rotor with the rotational speeds.

To evaluate the influence of mechanical losses such as that caused by friction in the bearings, the power coefficient could be further corrected as:

$$C_p = C_{p0} - \frac{b_L \overline{\omega^2}}{\frac{1}{2}\rho U_\infty^3 A}, \tag{15}$$

in which $b_L\omega^2$ represents mechanical losses. C_{p0} is the power coefficient without correction, *i.e.* the results with b_L=0, in this case all the hydrodynamic power is assumed being converted to mechanical power of the turbine.

The comparison between the power coefficient in the experiment conducted by Shiono *et al* (2000) and that predicted by the present numerical model is shown in Fig. 6. When b_L=0, the result of the forced rotating turbine predicts the maximum power efficiency is 29.4% at a tip-speed ratio 1.45, whilst the experiment

measured a maximum power efficiency of 20-23% at a tip-speed ratio 1.2-1.3. At first sight the discrepancy between prediction and measurement is remarkable, but if mechanical losses are taken into account the prediction are greatly improved. When b_L is set to 0.15, the predicted maximum power efficiency is 21.6% at a tip-speed ratio 1.25, agreeing very well with the experimental results. This is an example of how much the mechanical losses could affect the result. It should be noted that these mechanical losses are only accounted for in the model validation. This means that b_L is set to zero for all the results presented in Section 4.

The results of the hydrodynamic-driven turbine show similar variation with that of the forced rotating turbine, but the latter cannot give the fluctuation of the rotational speed, as well as the fluctuations of power and torque output. Therefore the hydrodynamic-driven method is applied for the simulations hereafter.

In the simulations for model validation the independence of the different parameters is also checked. The grid with nodes from around 100 thousand to more than 300 thousand, time increments Δt from 0.0001s to 0.003s and turbulent intensity on the inlet boundary from 1% to 5% are tested. It is found that the relative difference will be less than 5%, as long as the number of grid nodes is more than 200 thousand, the y^+ of grid points nearest to the blade is less than 2, and time increments $\Delta t \leq 0.002$s. The influence of turbulent intensity is negligible. The results shown in Fig. 6 (b) are calculated with Δt=0.0002s, turbulent intensity on inlet boundary 5%, and on a grid with 232617 nodes.

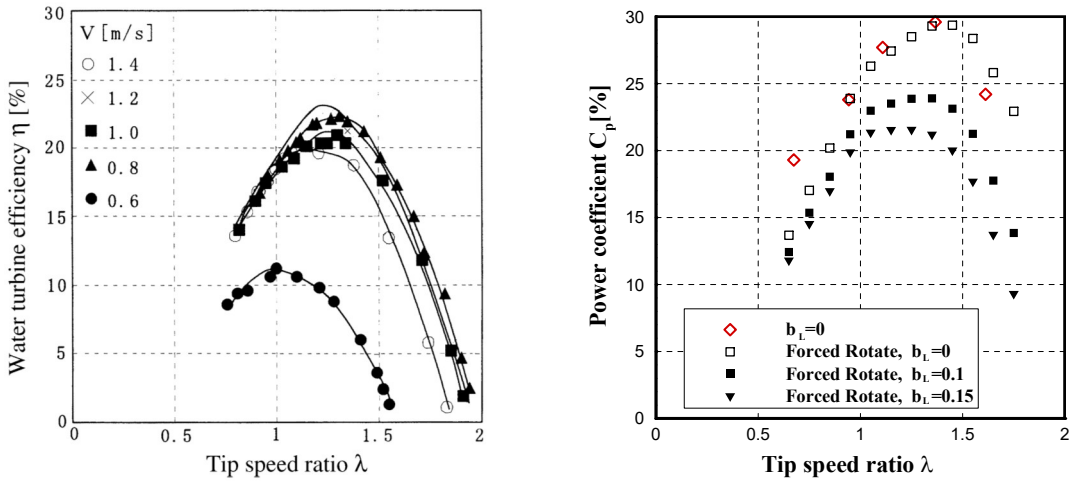

(a) Experimental results of Shiono *et al.* (2000). (b) Numerical results of present model.

Fig.6 Measured and computed power coefficient versus tip-speed ratio for a similar test case to the present one, σ=0.366.

4. Results and Discussions

4.1 Flow Field

Vorticity distributions around the rotor of the fixed-blade turbine predicted by the present model are shown in Fig. 7; the tip-speed ratio is 2.16 and Re_D is 10^6. The blades keep cutting through the wake of the blade ahead, like the blade is about to do at the bottom in Fig. 7. This phenomenon is apparent when λ>2. In this case, a DMS model cannot correctly predict the relative velocity experienced by a blade and an advance model, for example a RANS model, is necessary. The shed vortices move to the bottom side of the rotor; this is related to the rotating direction of the rotor. Fujisawa *et al* (2001) studied the flow field around a H-Darrieus turbine with Particle Image Velocimetry (PIV) in a water tunnel where the Reynolds number based on the diameter of the rotor ($Re_D=U_\infty D/\nu$) was 3×10^3 and the flow was laminar. Fujisawa *et al* (2001) report that the flow field is characterized by two pairs of vortices shed from the blade moving upstream, and suggest that the flow pattern is developed due to successive generation of separation on the inner surface of the blade followed by the formation of roll-up vortices from the outer surface. These mechanisms are observed in this simulation, too. Fig. 7 shows the separation on the inner surface of the bottom blade, and

the flow rolls up from the outer to the inner surface.

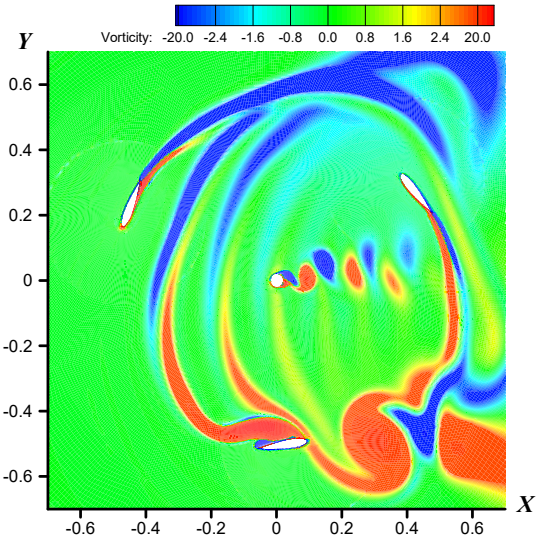

Fig.7 Predicted vorticity distribution around the rotor, λ=2.16. Ambient flow comes from the left.

4.2 Angle of Attack

The cyclic variation of angle of attack of vertical-axis turbine blades is responsible for the fluctuations in hydrodynamic forces on the blades. Especially at low tip-speed ratio the angle of attack could exceed the stall angle, and lead to large periodic variation of hydrodynamic loads on the blades. It may cause serious vibrations and risk the structures to fatigue damage, which is one of the most criticized drawbacks of VAT's. It is necessary to compare the blades' angle of attack of fixed pitch and variable pitch turbines. If the flow crossing the upstream half rotor is assumed undisturbed, then the angle of attack α is a function of the azimuthal angle θ, the pitch angle φ, and the instantaneous non-dimensionalized rotational speed λ' of the rotor, namely

$$\alpha = \alpha_{fix} - \varphi = \arctan\left(\frac{\sin\theta}{\lambda' + \cos\theta}\right) - \varphi, \tag{16}$$

in which α_{fix} is the angle of attack of a reference fixed pitch blade. Fig. 8 shows the phase averaged variations of angle of attack α and lift coefficient C_L of Blade #1 at upstream half cycle of the rotation in the case of tip-speed ratio λ=2.10 and amplitude of pitch variation φ_{amp}=10°. Blade #1 is the blade located at the positive y axis when $\theta = 0$ (cf. Fig. 1). The non-dimensionalized rotational speed λ' and the α_{fix} are also presented in the figure for reference. In the figure T is the period of revolution. t/T=0.25 can be regarded as the most upstream point and t/T=0.5 the division point of upstream and downstream half cycles of rotation, though they are not the exact points since the rotational speed is not constant. The lift coefficient C_L is defined as:

$$C_L = \frac{F_{lift}}{\frac{1}{2}\rho V_r^2 C}, \tag{17}$$

in which V_r is the flow speed relative to the blade; F_{lift} is the lift acting on the blade, it is orthogonal to the relative velocity and is positive when pointing inside the rotor. V_r and F_{lift} need to be derived considering the geometric relations among vectors of the ambient flow velocity, the blade's motion, and the hydrodynamic forces on the blade; the details of these relations are omitted here for brevity. The reason that only the α and the C_L at upstream half cycle are presented is: the flow past the upstream half rotor has been disturbed very much by the wakes created by blades and shaft, the assumption of undisturbed ambient

flow reluctantly accepted at upstream half rotor are no longer valid; in addition, the contribution of downstream half cycle to the driving torque are very small as will be explained later.

It is shown in the figure that the angles of attack exhibit double peaks due to the fluctuation in rotational speed. The actual angle of attack α is lower than α_{fix}, the difference between them is the pitch angle of the blade as regulated by Eq. (16). Therefore the maximum α occurs close to the end of the upstream half cycle whilst the maximum α_{fix} occurs close to the most upstream point. The curve of C_L jumps down at both ends close to t/T=0 and 0.5, when the lift is about to change its directions abruptly. When t/T≈0.42 at the angle of attack 16.5°, C_L reaches up to 2.42. In the range of blade Reynolds number of this simulation, the static stall angle of NACA0018 airfoil is around 10° and the maximum C_L is around 1.0. The dynamic stall angle and the maximum lift coefficient well exceed their static values. After the lift coefficient reaches the peak, it decreases when the angle of attack decreases.

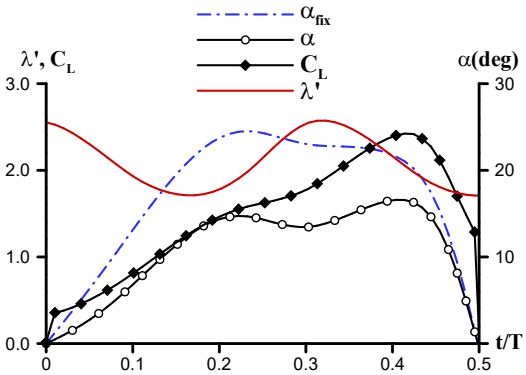

Fig.8 Phase-averaged angle of attack, non-dimensional rotational speed and C_L at upstream half cycle, λ=2.10, φ_{amp}=10°.

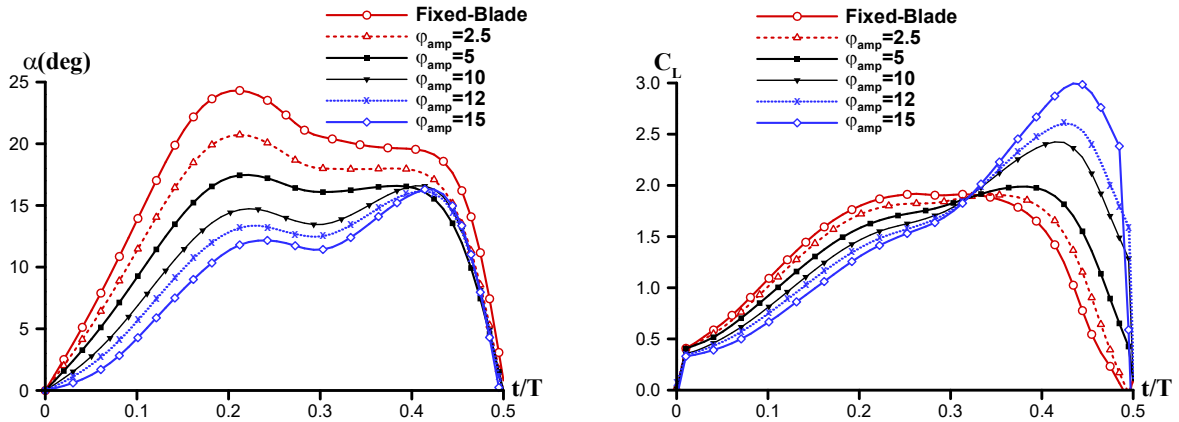

(a) Angle of attack. (b) Lift coefficient.

Fig. 9 Phase-averaged angle of attack and lift coefficient at the upstream half cycle, λ=1.93~2.16

Fig. 9 shows the comparison of phase-averaged variations of angle of attack α and lift coefficient C_L of Blade #1 at upstream half cycle in the case of different amplitudes of pitch variation. The comparison should be made at the same tip-speed ratio, but it is hard to obtain a specific tip-speed ratio by adjusting the load coefficient. Instead, all tip-speed ratios for the data in the figure are approximately 2.0; the maximum is 2.16 in the case of fixed blade turbine, and the minimum is 1.93 in the case of φ_{amp}=15°. The optimum tip-speed ratio λ_{opt} is 2.0 for all cases except for the case of φ_{amp}=15° where λ_{opt} is much lower as displayed in Fig. 10 (a). Two general trends in the figure seems fairly clear, although it is inappropriate to compare a curve directly to another because of the difference in average tip-speed ratios. The first is the angles of attack are decreased and their local peaks around t/T≈0.2 are postponed with increasing φ_{amp}; this directly shows the effect of variable pitch on reducing the angle of attack. The second is with increasing φ_{amp}, the lift coefficient decreased when t/T<0.32 and increased when t/T>0.32. Especially the maximum C_L is

remarkably increased in the latter case, although at these azimuth positions the magnitudes of V_r are relatively small, the large C_L does not necessary mean large lift force. The variation of lift coefficients could be explained as: the blades with smaller pitch angle reach the peak of angle of attack more quickly, so their lift coefficients increase more quickly either; but for the blades which can increase angle of attack further or reach an even higher peak, a much higher maximum C_L can be created. Dynamic effects play important role in this situation since both angle of attack and the lift coefficient well exceed their static stall angle and maximum lift coefficient.

4.3 Overall Output of the Turbine

The variation of power output characteristics of a fixed-blade turbine and of a variable pitching blades VAT with φ_{amp} ranging between 2.5° and 15° are shown in Fig. 10. By gradually increasing the load coefficient b in Eq. (2), the tip-speed ratio of the turbine decreases. Figure 10 (a) shows that the maximum power coefficient for a fixed-blade turbine is 0.27. Numerical simulations of a similar turbine, but four times larger in size and with a free-stream speed of 1.5m/s (Chen *et al.*, 2017), predicted a maximum power coefficient of 0.45, much higher than that in this study. For a tip-speed ratio of 2, the blade Reynolds number is around 3×10^5 in this paper and 2×10^6 in Chen *et al.* (2017). According to Paraschivoiu (1998), the stall angle of the NACA0018 airfoil at Re_b=3.6×10^5 is 12° where the lift and drag coefficients at this angle are 0.93 and 0.024, respectively. At Re_b=2×10^6, the stall angle and corresponding lift and drag coefficients are 14°, 1.18 and 0.02, respectively. This has a major effect on VAT's as they operates both in pre-stall and post-stall conditions.

Figure 10 shows that when the amplitude of pitch variation is 2.5°, the maximum power coefficient C_{pmax} is 0.33, which is 22% higher than that of the fixed-blade turbine. When φ_{amp} increases to 5°, C_{pmax} further increases to 0.36, 33% higher than that of the fixed-blade turbine. In these conditions, the optimum tip-speed ratio λ_{opt} is about 2.0. When φ_{amp} increases to 10°, C_{pmax}=0.37 and λ_{opt} =1.8. When φ_{amp} increase further to 12° and 15°, C_{pmax} decreases.

The peak of the C_p-λ curve becomes sharper and sharper with the increase of φ_{amp}. All the C_p-λ curves collapse at lower tip-speed ratio. It means the hydrodynamic efficiency is independent of the blade pitch at low tip-speed ratio. On the other hand, the benefit of variable pitching diminishes at very large tip-speed ratios, because the angle of attack variations experienced by the fixed blade are small. Moreover, in the cases of high φ_{amp} (10°, 12°, and 15°), the range of tip-speed ratio that allows high C_p decreases. For the flow conditions and turbine characteristics investigated, the optimum amplitude of sinusoidal pitch variation is 5°-10°.

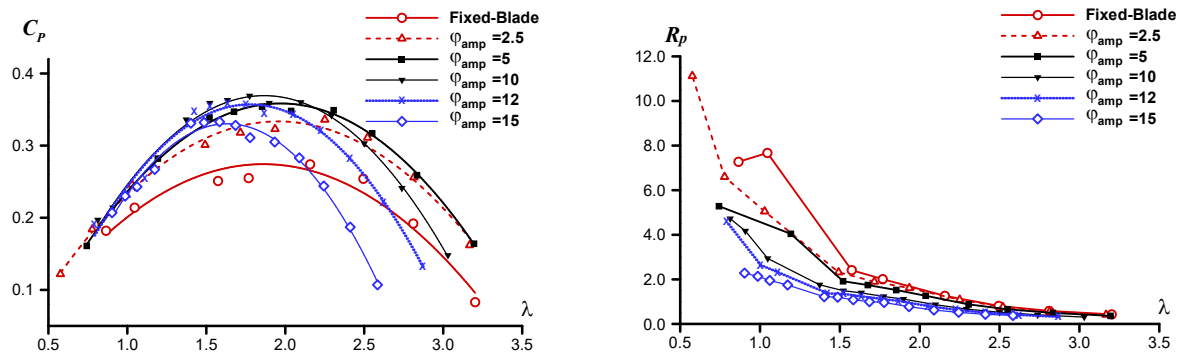

(a) Power coefficient versus tip-speed ratio. (b) Ripple factor of power output versus tip-speed ratio.

Fig.10 Power coefficient versus tip-speed ratio.

Fig. 10 (b) is the ripple factor of power output R_P. The ripple factors are very high and also scattered at low tip-speed ratio. The reason for this is shown in Fig. 11, where the time series of non-dimensionalized power output, rotation speed, and azimuth angle are shown. At high tip-speed ratios, the load on the shaft

is not very high, the resistant torque balances the driving torque; the blades hardly experience stall and the turbine operates in a smooth periodic manner. For example, the time series of all variables in each cycle of rotation exhibit good periodicity at λ=1.85 in Fig. 11 (a). Conversely, at low tip-speed ratios, *e.g.* λ=0.74 as in Fig. 11 (b), the turbine rotates discontinuously, sometimes suddenly accelerating and sometime stagnating for a while, or even rotating backwards occasionally. This phenomenon could be observed in flume experiments when the turbine is not fully started up, or the load on the shaft is too high.

The hydrodynamic torque (Q_H) and the load torque (Q_L) are of similar amplitude and, thus, the net torque is small (cf. Eq. 1). Every time one blade passes through the most upstream point of the rotor, the rotational speed (ω) reaches its maximum and the load torque reaches its minimum ($Q_L = -b\omega$). Past this azimuthal position, the hydrodynamic torque decreases abruptly while the rotor takes some time to decelerate. Therefore, the load torque becomes larger than the hydrodynamic torque resulting in a negative net torque (Q_H+Q_L). The rotor then reaches a minimum rotational speed, which can be negative. At this point, however, the resistant torque is small (and could also be positive), and thus the net driving torque restarts the rotor. The hydrodynamic torque increases smoothly until the next blade approaches the most upstream point. This results in sharp peaks of the curves of power output and rotational speed, as shown in Fig. 11 (b). The narrow peaks and the close to zero values in the remaining parts of a cycle, lead to small mean values and large ripple factors. It is important to note that if the turbine was set to rotate at a predetermined speed, as in most numerical simulations in the literature, this phenomenon could not have been observed.

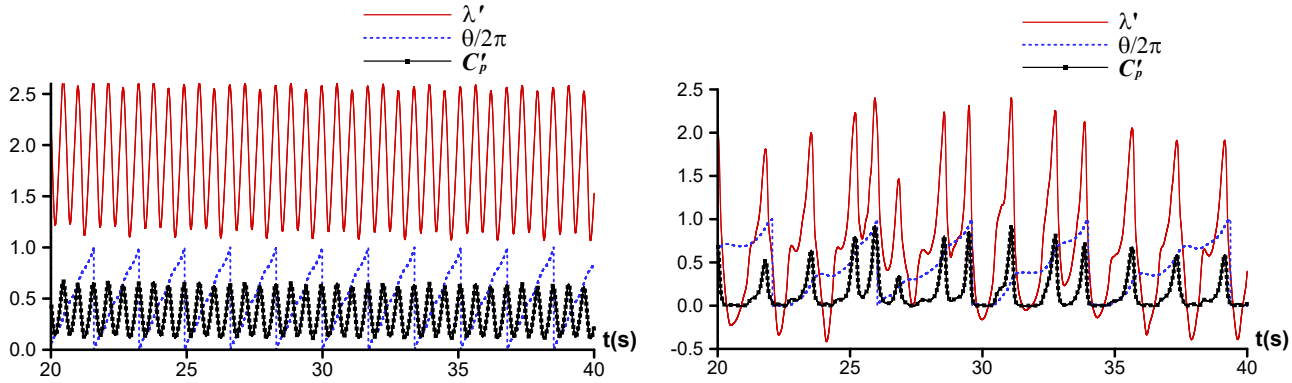

(a) λ=1.85 (b) λ=0.74

Fig.11 time series of non-dimensionalized rotation speed, azimuth angle, and power output, φ_{amp}=5°

If the blades are pitched, the stall behavior is improved significantly at low tip-speed ratios, so that R_P decreases when φ_{amp} increases. But at high tip-speed ratios, the effect of variable pitch is not significant and all R_P curves collapse to 0.3 for λ>3. At a tip-speed ratio equal to 2.0, around which the fixed-blade turbine and variable pitch turbines with φ_{amp}≤5° achieve maximum power efficiency, R_P is 1.56 and 1.32 for fixed pitch and φ_{amp}=5°, respectively. Therefore, the variable pitch allows an R_P reduction of 15%.

The ripple factor of rotational speed R_ω also decreases when φ_{amp} increases, its variation is very similar to that of R_P based on the relation between rotational speed and power output given by Eq.(9). The ripple factor of torque on the shaft is exactly equal to the ripple factor of rotational speed, because the torque on the shaft is equal to the rotational speed multiplied by a constant load coefficient. Therefore, the figures of those ripple factors are omitted.

The time-averaged torque coefficient on the shaft $\overline{C_q}$ is shown in Fig. 12. The comparison between Fig. 10 (a) and Fig. 12 shows that the torque coefficient is maximum at a lower tip-speed ratio than that where the power coefficient is maximum. This is because the power coefficient is proportional to the square

of the rotational speed, while the torque coefficient varies linearly with the rotational speed.

Note that because ω>1, then $\overline{\omega^2}$ is larger than $\overline{\omega}^2$, and the larger the ripple of ω, the larger the difference between them. As a result, $\overline{C_q}$ is lower than the ratio of C_P over λ according to Eqs. (8), (10) and (11). It has been shown that R_ω decreases as φ_{amp} increase, especially at low λ. Therefore, at low λ, the larger the φ_{amp}, the smaller R_ω and the larger $\overline{C_q}$.

At tip-speed ratio 2.0, the time-averaged torque coefficient on the shaft of the fixed-blade turbine is 0.125, and that of a variable pitch turbines with φ_{amp}=5° is 0.173, which is 38% higher than that of a fixed-blade turbine.

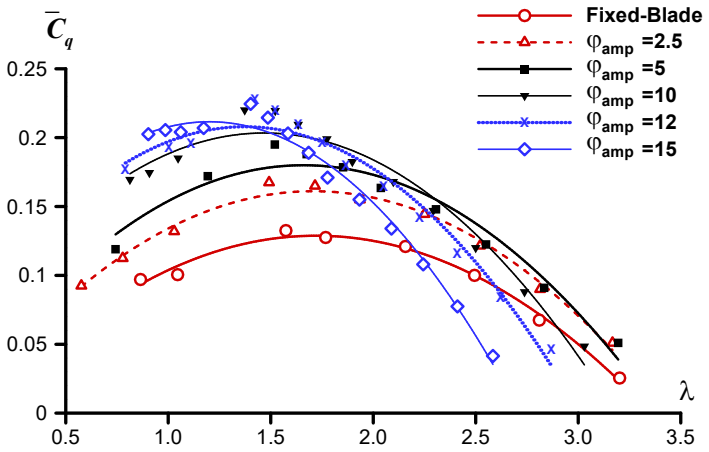

Fig. 12 Time-averaged torque coefficients

4.4 Characteristics of Hydrodynamic Loads on Blades

Similar to the definition of the torque coefficient (Eq. 14), let us define the coefficient of hydrodynamic torque acting on a blade as:

$$C_{qb} = \frac{Q_b}{\frac{1}{2}\rho U_\infty^2 DHR}, \tag{18}$$

where Q_b is the hydrodynamic torque acting on the blade. The coefficients of tangential and normal hydrodynamic forces acting on a blade are defined as

$$CF_{Tb} = \frac{F_{Tb}}{\frac{1}{2}\rho U_\infty^2 cH}, \qquad CF_{Nb} = \frac{F_{Nb}}{\frac{1}{2}\rho U_\infty^2 cH}, \tag{19}$$

where F_{Tb}, F_{Nb}, are the tangential and normal hydrodynamic forces as shown in Fig. 1. The normal force is positive when it points inwards on the rotor; the tangential force is positive anticlockwise. Note that the definition of the force coefficients adopted here is different from the conventional definition of the aerodynamic coefficients of airfoils, because the characteristic speed used here is the undisturbed flow speed instead of the relative flow speed experienced by the blade section.

The time series of hydrodynamic torque coefficients on the three blades and on the whole rotor, as well as the hydrodynamic force coefficients on the blades of the variable pitch turbine, are shown in Fig. 13. Blades #2 and #3 are the blades whose azimuth angles are 120° and 240° ahead of blade #1, respectively. As typical of VAT's, the torque and force coefficients are positive and relatively large on a blade in the

upstream half cycle ($0<\theta<\pi$ for blade #1), while in the downstream half cycle they are small or even negative. The hydrodynamic torque on the rotor is the sum of that on the three blades. The fluctuation in hydrodynamic torque on the rotor is much lower than that on an individual blade due to the phase difference between blades. As a typical example, the data for φ_{amp}=5° and λ=2.04 are shown. The peaks of hydrodynamic torque coefficient on the rotor is always corresponding to a peak of hydrodynamic torque coefficient on a blade. The maximum torque coefficient on the rotor is much lower, 75% in this case, than that on a blade; whilst the fluctuation in torque coefficient on the rotor is only half of that on a blade. The torque and force coefficients are periodic at a high tip speed ratio of 2.04. The periodicity is broken when $\lambda\leq$1.2 for fixed blades and for $\varphi_{amp}\leq$5°, while at lower tip-speed ratios ($\lambda\leq$1.0) the breakdown occurs at φ_{amp}=10° and 12°. For φ_{amp}=15°, periodicity is maintained for λ as low as 0.9.

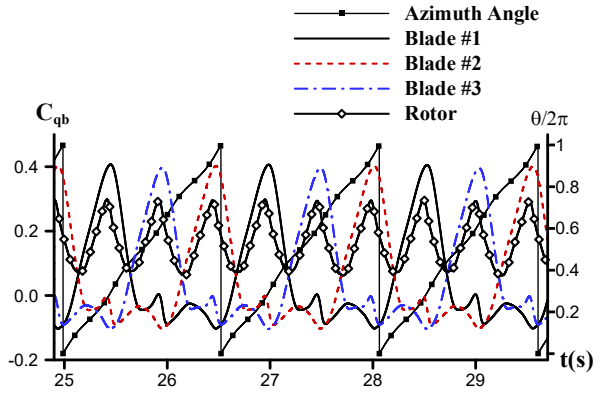

(a) Hydrodynamic torque coefficient for the 3 blades and the rotor

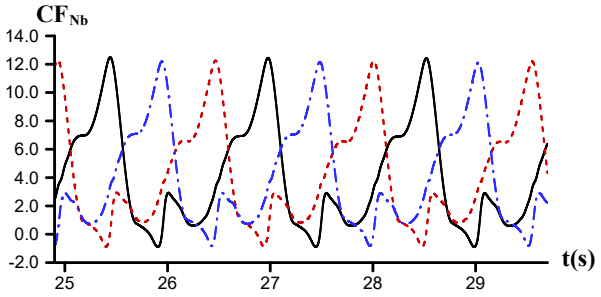

(b) Normal force coefficient for the 3 blades

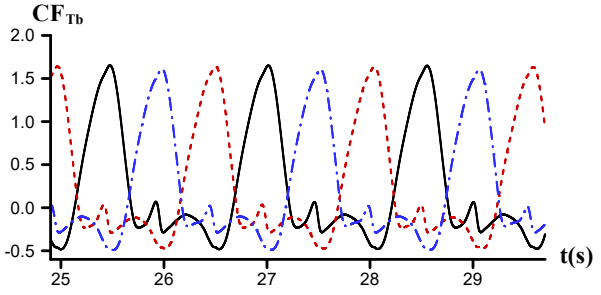

(c) Tangential force coefficients for the 3 blades

Fig. 13 Hydrodynamic force and torque coefficients for variable pitch turbine over 5 s, λ=2.04, φ_{amp}=5°.

The comparison of phase-averaged hydrodynamic torque coefficients of different φ_{amp} are shown in Fig. 14. In the upstream half cycle, the maximum hydrodynamic torque coefficient of all curves occurs at $t/T\approx$0.3, *i.e.* $\theta\approx$108°. The maximum coefficients of different variable pitch turbines are close to each other's, and they are larger than that of the fixed-blade turbine. Most of the times, the curves of the variable pitch turbines are above that of the fixed-blade turbine. In the downstream half cycle, the coefficients are

predominately negative. The magnitude of the negative coefficients of φ_{amp}=10°-15° is larger than that of $\varphi_{amp}\leq$5°. The comparison reveals that the benefits of variable pitching are gained mainly from the upstream half cycle, where the blades are kept working in pre-stall regime for as long as possible.

Regarding the turbine as a double actuator disk, the kinetic energy of the free stream flow is extracted by the upstream actuator disk, thus the velocity within the rotor is smaller than that of the free stream, and the velocity at the exit of the rotor is even smaller than that inside. As a consequence, the local tip-speed ratio on the downstream half of the rotor is larger than that on the upstream half. The more efficient the upstream half rotor is, the more prominent is this effect. When the local tip-speed ratio of the downstream half rotor is large, the benefit of variable pitching decreases. If the blades are forced to pitching over an appropriate angle, it may even cause resistant torque, as in the cases of $\varphi_{amp}\geq$10° in Fig. 14. This also results in the quick drop of the power coefficient curves in Fig. 10 (a) when $\varphi_{amp}\geq$10° at high tip-speed ratio.

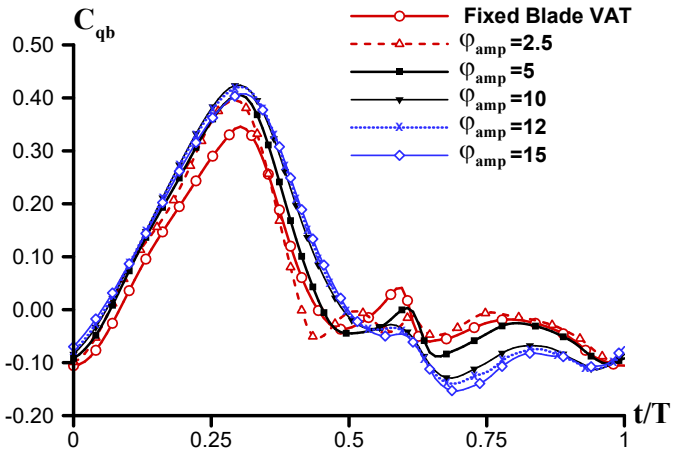

Fig. 14 Phase-averaged hydrodynamic torque coefficients on the blades over a period of revolution, λ=1.93~2.16

The phase-averaged hydrodynamic force coefficients on a blade are shown in Fig. 15. In the upstream half cycle, the larger the φ_{amp}, the smaller is the maximum tangential force coefficient and the later the maximum takes place. As Paraschivoiu (1982) showed with a multiple streamtube model, the angle of attack reaches a maximum at 0.25<t/T<0.5. Usually the hydrodynamic force has a local maximum around the stall angle, the delay of maximum coefficient is due to the stall delay enabled by the variable pitch. The decrease of relative flow speed experienced by the blade also contributes to decrease the maximum coefficient. In the downstream half cycle, especially when t/T>0.6, the differences in the tangential force coefficients are smaller than in the upstream half cycle. This is again due to the relatively large local tip-speed ratio on the downstream half of the rotor.

The maxima of normal force coefficients decrease and occur slightly later in phase as φ_{amp} increases.

The larger the φ_{amp}, the longer the arm of the normal force, as clearly revealed by Fig. 1. Therefore, although the normal force on variable pitching blades is lower than that on a fixed blade, the increased arm results in larger torque. Figures 14 and 15 show that, at φ_{amp}=5°, while the maximum torque coefficient is 117% of that of the fixed-blade turbine, the maximum tangential and normal force coefficients are only 72% and 86% of that of the fixed-blade turbine, respectively.

An actuator disk type model always predicts a negative normal force in the downstream half of the rotor, *i.e.* the force points outwards of the rotor as long as the induced velocity on the downstream disk is in the direction of the free-stream flow. However, Fig. 15 (b) shows that for the majority of the downstream half cycle, the normal force coefficient is positive even in the case of the fixed-blade turbine. A positive normal force in the downstream half cycle creates a resistant torque in the cases of sinusoidal pitching blades. Therefore, the relatively larger positive normal force coefficient with $\varphi_{amp}\geq$10° is associated with the larger

resistant torque at t/T>0.6 as shown in Fig. 14.

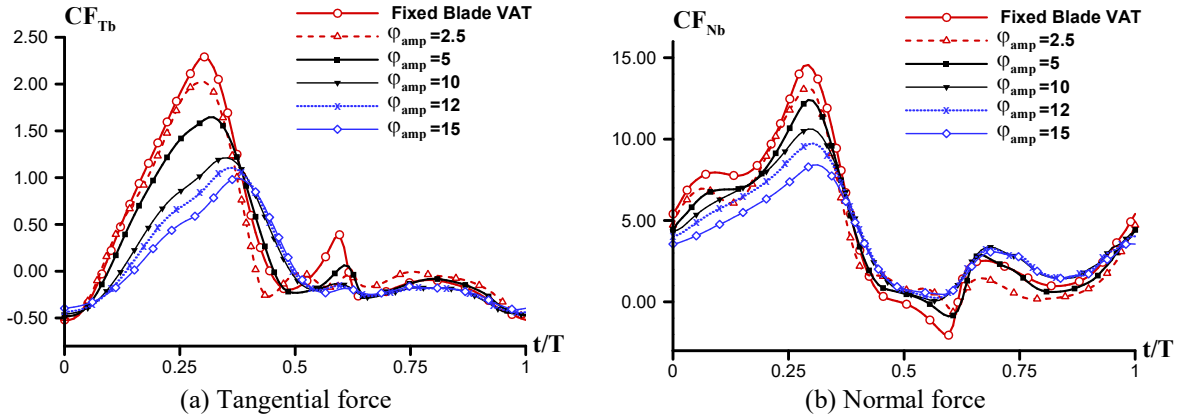

(a) Tangential force (b) Normal force

Fig. 15 Phase-averaged hydrodynamic force coefficients on the blades over a period of revolution, λ=1.93~2.16

Variations of the maximum tangential ($CF_{Tb.max}$) and normal ($CF_{Nb.max}$) force coefficients are shown in Fig. 16. Both $CF_{Tb.max}$ and $CF_{Nb.max}$ decrease with increasing amplitude of pitching. All the normal force coefficient curves have a local minimum around their optimum tip-speed ratio, *i.e.* λ=1.5~2, after that $CF_{Nb.max}$ increases monotonously with the increase of tip-speed ratio. For variable pitch turbines, $CF_{Tb.max}$ decreases with increasing tip-speed ratio. For the fixed-blade turbine, there is no simple correlation between $CF_{Tb.max}$ and the torque coefficient on the shaft C_q. The latter is related to the sum of the hydrodynamic torques on all three blades, and thus it is affected by not only an instantaneous maximum tangential force but also by its variation over the whole rotation cycle. In addition, the length of arm for normal force increases with φ_{amp}. A kinematic analysis indicates that when φ=10°, the driving torque created by the normal force is equivalent to that due to the tangential force as long as the ratio of the normal force over the tangential force is close to 6. Comparing Fig. 16 (a) and (b), this ratio is reached as early as λ=1.5. For φ=5° the ratio needs to be more than 11; although this criterion is not reached at λ=2.0, the torque created by the normal force is still comparable to that by the tangential force. Therefore, with lower tangential and normal forces, the blades of a variable pitch turbine can still create higher driving torque than that of a fixed-blade turbine.

Curves of the amplitude of tangential ($CF_{Tb.amp}$) and normal ($CF_{Nb.amp}$) force coefficients are shown in Fig. 17. Both $CF_{Tb.amp}$ and $CF_{Nb.amp}$ decrease with increasing pitch amplitude. The amplitude of the tangential force coefficient does not change significantly for tip-speed ratios higher than the ideal one. Conversely, $CF_{Nb.amp}$ is minimum at the optimum tip-speed ratio, and this implies that the turbine always reaches highest efficiency when its blades experience the most stable hydrodynamic forces.

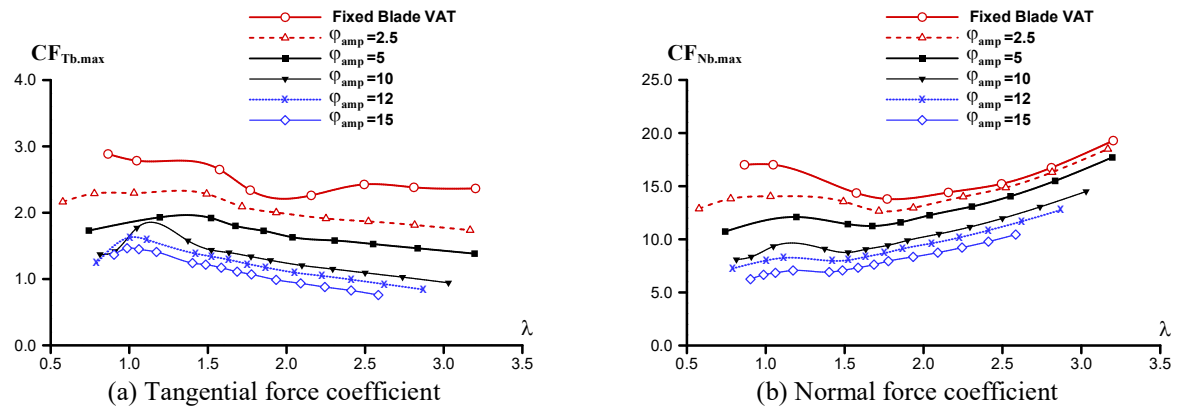

(a) Tangential force coefficient (b) Normal force coefficient

Fig. 16 Maximum phase-averaged force coefficient on a blade versus the tip-speed ratio.

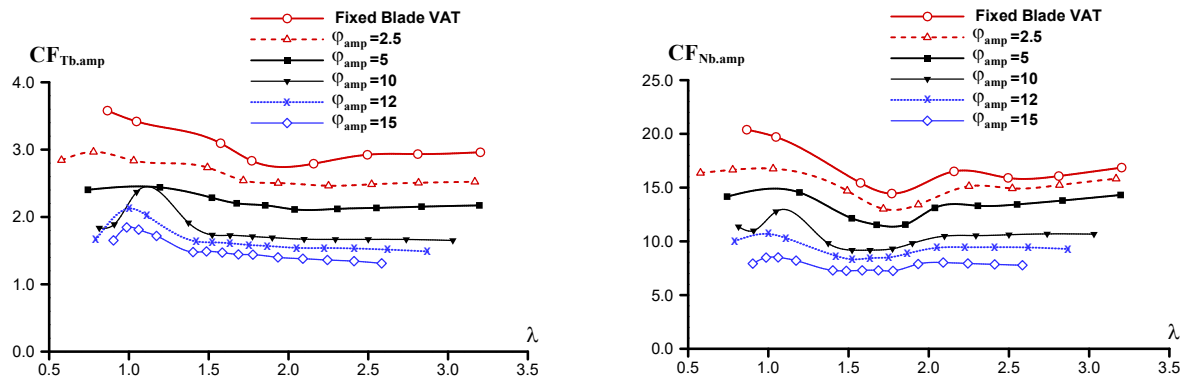

(a) Tangential force coefficient (b) Normal force coefficient

Fig. 17 Amplitude of the phase-averaged force coefficient variation on a blade versus the tip-speed ratio.

4.5 Influence of Rotor Parameters

A higher inertia makes the rotor rotation more stable, though it usually implies heavier components and difficulties in delivering; a lower rotor solidity makes the rotor rotation faster, as long as the relative velocity between the blades and the water do not exceed the limitation to avoid cavitation.

To evaluate the influence of inertia of the rotor, running the rotor with twice and three times larger inertia are simulated. Both fixed-blade turbines, and with φ_{amp}=10° the only representative for variable pitch turbines, are simulated. The tip-speed ratios for the fixed-blade turbine and variable pitch turbine at original inertia are 2.16 and 2.10, respectively. They are chosen because their tip-speed ratios are close to each other and close to the optimal tip-speed ratio at the same time. The results of power coefficient C_p, tip-speed ratio λ, ripple factors of power output R_p and of rotational speed R_ω, are shown in Fig. 16. When inertia of rotor is three times larger, C_p and λ are slightly increased, and the ripple factors R_p and R_ω are apparently decreased. For variable pitch turbines the increases of C_p and λ are less than 2%, R_p and R_ω are 55% of the original values; for fixed-blade turbine the increases of C_p and λ are less than 5%, R_p and R_ω are 50% of the original values.

The results shows that the influence of inertia on the average characteristics such as power coefficient and tip-speed ratio are very small, but larger inertia does make the turbine run more stable. The effects of larger inertia on both fixed and variable pitch turbines are quite similar, so the discussions on the comparisons between fixed and variable pitch turbines in previous sections are not affected much by the inertia of the rotor.

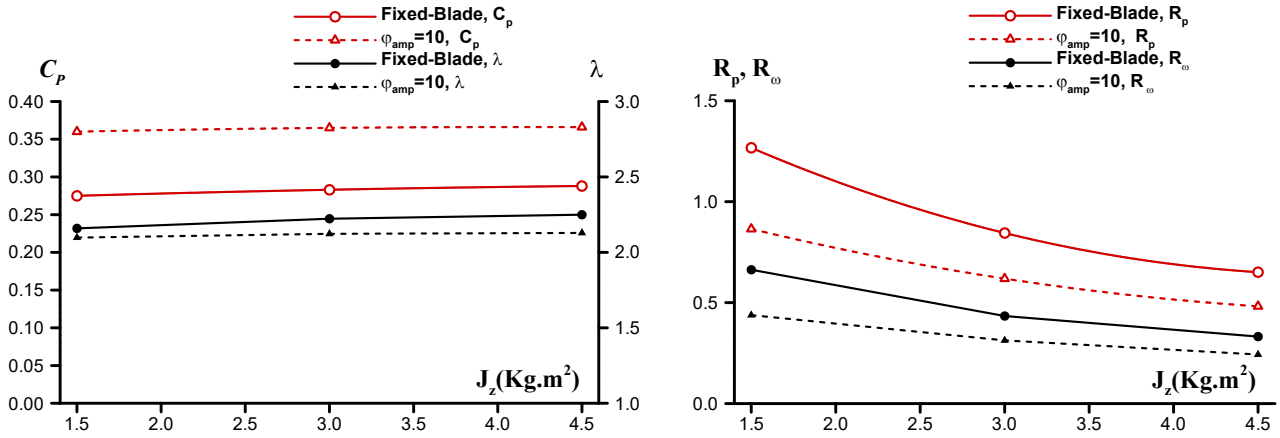

(a) Power coefficient and tip-speed ratio (b) Ripple factors of power output and rotational speed

Fig. 16 Influence of inertia of rotor.

A few simulations of rotor with solidity, only half of that in Table 1, are conducted. For both fixed and variable pitch turbine, the optimal tip-speed ratio of the half solidity turbine is around 3.3. A load coefficient 1/2 of the original turbine must be used to give a 15% higher maximum power coefficient than the original fixed-blade turbine. Compared to a fixed-blade turbine, the variable pitching with φ_{amp}=2.5° improves the power output further by 10~15%, but with φ_{amp}=5° makes the performance worse than the fixed-blade turbine. Unlike the effect of inertia of rotor, different solidity makes a total new series of turbines. These simulations suggest that the tendency of performance improvement due to variable pitching for lower solidity turbines is similar with that for present turbines. The performance of the fixed-blade turbine with lower solidity could be better than that with higher solidity, but the degree of performance enhancement by variable pitching decrease because there is always a limit for turbine performance.

5. Conclusions

Numerical simulations are carried out to compare the performances of a vertical-axis turbine with fixed and sinusoidal pitch of the blades. The Reynolds-averaged Navier-Stokes equations are solved with a finite-volume solver, where the shear stress transport k-ω turbulence model is used for closure. The output characteristics of fixed and variable pitch turbines with different amplitude of pitching are compared; power coefficient, torque coefficient, ripple factors, hydrodynamic torques, tangential and normal forces on a blade are considered. In this study, the variable pitch is investigated not for a constant angular velocity of the turbine, but for a more-realistic, variable, angular velocity. This is computed solving the equation of motion and accounting for a torque resistance proportional to the angular velocity. The following conclusions are drawn:

(1) The optimum tip-speed ratio is about 2 for the fixed pitch turbine in this paper. Sinusoidal pitching significantly improves the characteristics of power efficiency and torque output of the turbine without changing the optimum tip-speed ratio. Compared to the fixed pitch turbine, the maximum power efficiency and torque output of variable pitch turbine are more than one thirds higher whilst the fluctuations in power output and rotational speed are much lower.

(2) The benefits of variable pitching are gained mainly in the upstream half cycle of the blades' path, where it delays stall. Due to the high *local* tip-speed ratio in the downstream half cycle, a pitch amplitude that is too high leads to a resistant torque that nullifies the benefits gained in the upstream half cycle. There is an optimum amplitude of sinusoidal pitch variation for a given turbine, which lies in 5°-10° for the conditions tested in this paper.

(3) In the case of variable pitch turbines, both forces tangential and forces normal to the blade chord contribute to the driving torque. Therefore, although the tangential and normal forces on variable pitching blades are significantly lower than those on a fixed blade, the effect of increased arm of force still creates larger driving torque.

(4) The above conclusions have been verified for a wide range of inertia of rotation. For turbines with lower rotor solidity that runs faster, a smaller amplitude of pitch variation is required and the benefit gained from variable pitching is less significant.

The present results should be used with care because three-dimensional effects, including those due to the arms and the finite length of the blades, would lead to a reduction in the turbine efficiency.

Acknowledgement

This work is supported by the general program from the Natural Science Foundation of China (NSFC) with grant No. 51379036. The calculations were performed on the supercomputer TianHe-1A at the

National Supercomputer Center in Tianjin, China.

References

Chen, B, Cheng, SB, Su, TC, and Zhang, H (2017) "Numerical Investigation of a Vertical-axis Tidal Turbine in a Channel," submitted to *Ocean Engineering*.

Chougule, P, and Nielsen, S (2014), "Overview and design of self-acting pitch control mechanism for vertical axis wind turbine using multi body simulation approach," *Journal of Physics: Conference Series*, 524(2014):012055.

Coiro, DP, De Marco, A, Nicolosi, F, Melone, S, and Montella, F (2005), "Dynamic behavior of the patented Kobold tidal current turbine: numerical and experimental aspects," *Acta Polytechnica*, 2005, 45(3):77-84.

Erickson, DW, Wallace, JJ, and Peraire, J (2011), "Performance characterization of cyclic blade pitch variation on a vertical axis wind turbine", *Proceedings of 49th AIAA Aerospace Science Meeting including the New Horizons Forum and Aerospace Exposition,* January 4-7, 2011, Orlando, Florida.

Fujisawa, N, and Shibuya, S (2001), "Observations of dynamic stall on Darrieus wind turbine blades," *Journal of Wind Engineering and Industrial Aerodynamics*, 89(2001): 201-214.

Gorlov, A (1995), "The helical turbine: a new idea for low-head hydropower," *Hydro Rev.*, 14(5): 44-50.

Gorlov, A (1998), "Development of the helical reaction hydraulic turbine," *Final Technical Report* (DE-FGO1-96EE 15669) to The US Department of Energy, August, 1998.

Gosselin, R (2015), *Analysis and Optimization of Vertical Axis Turbines*, PhD thesis, Université Laval, Québec, Canada.

Gosselin, R, Dumas, G, and Boudreau, M (2016), "Parametric study of H-Darrieus vertical-axis turbines using CFD simulations," *Journal of Renewable and Sustainable Energy*, Vol 8, 053301-1~22, 2016.

Grylls, W, Dale, B, and Sarre, PE (1978), "A theoretical and experimental investigation into the variable pitch vertical axis wind turbine," *Proc. 2nd Int. Symposium on Wind Energy Systems*, Oct. 3-6, 1978, Amsterdam, Netherlands, pp. E9-101-E9-108.

Hantoro, R, Utama, IKAP, Erwandi, and Sulisetyono, A (2011), "An experimental investigation of passive variable-pitch vertical-axis ocean current turbine," ITB J. Eng. Sci., 43(1): 27-40.

Hwang, IS, Lee, YH, and Kim, SJ (2009), "Optimization of cycloidal water turbine and the performance improvement by individual blade control", *Applied Energy*, 86 (2009):1532-1540.

Kirke, BK and Paillard, B (2017), "Predicted and measured performance of a vertical axis wind turbine with passive variable pitch compared to fixed pitch," *Wind Engineering*, 41(1):74-90.

Kirke, BK and Lazauskas, L (1991), "Enhancing the performance of a vertical axis wind turbine using a simple variable pitch system," *Wind Engineering*, 15(4):187-195.

Kirke, BK and Lazauskas, L (1993), "Experimental verification of a mathematical model for predicting the performance of a self-acting variable pitch vertical axis wind turbine," *Wind Engineering*, 17(2): 58-66.

Kirke, BK and Lazauskas, L (2008), "Variable pitch Darrieus water turbines," *Journal of Fluid Science and Technology*, 3(3): 430-438.

Kirke, BK and Lazauskas, L (2011), "Limitations of fixed pitch Darrieus hydrokinetic turbines and the challenge of variable pitch," *Renewable Energy*, 36(2011): 893-897.

Lazauskas, L (1992), "Three pitch control systems for vertical axis wind turbines compared," *Wind Engineering*, 16(5):269-281.

Lazauskas, L and Kirke, BK (2012), Modeling passive variable pitch cross flow hydrokinetic turbines to maximize performance and smooth operation," *Renewable Energy*, 45(2012): 41-50.

Li, Y and Calisal, S M (2010), "Three-dimensional effects and arm effects on modeling a vertical axis tidal current turbine." *Renewable Energy*, 2010, 35:2325-2334.

Marsh, P, Ranmuthugala, Dev, Penesis, I, Thomas, G (2015), "Three-dimensional numerical simulations of straight-bladed vertical axis tidal turbines investigating power output, torque ripple and mounting forces," *Renewable Energy*, 83:67-77.

Miau, JJ, Liang, SY, Yu, RM, Hu, CC, Leu, TS, Cheng, JC, and Chen, SJ (2012), " Design and test of a vertical-axis wind turbine with pitch control," *Applied Mechanics and Materials*, 225(2012): 338-343.

Paillard, B, Hauville, F, and Astolfi, JA (2013), "Simulating variable pitch crossflow water turbines: A coupled unsteady ONERA-EDLIN model and streamtube model," *Renewable Energy*, 52(2013): 209-217.

Paraschivoiu, I (1998), *Aérodynamique Subsonique*, Presses Internationales Polytechnique, Montréal.

Paraschivoiu, I (1982), "Aerodynamic loads and performance of the Darrieus rotor," *AIAA Journal of Energy*, 6(6): 406-412.

Paraschivoiu, I, Trifu, O and Saeed, F (2009), "H-Darrieus wind turbine with blade pitch control," *International Journal of Rotating Machinery*, Vol 2009, doi:10.1155/2009/50543.

Salter, S (2005), "Pitch-control for vertical-axis, marine-current generator," *World Renewable Energy Conference Aberdeen 2005*.

Salter, SH and Taylor, JRM (2007), "Vertical-axis tidal-current generators and the Pentland firth," *Proceedings of the Institution of Mechanical Engineers, Part A: Journal of Power and Energy*, March 2007, 221: 181-199.

Schönborn, A, and Chantzidakis, M (2007), "Development of a hydraulic control mechanism for cyclic pitch marine current turbines," *Renewable Energy*, 32(2007): 662 – 679.

Shiono, M, Suzuki, K and Kiho, S (2000), "An experimental study of the characteristics of a Darrieus turbine for tidal power generation," *Electrical Engineering in Japan*, 2000, 132(3): 38–47.

Staelens, Y, Saeed, F, and Paraschivoiu, I (2003), "A straight-bladed variable-pitch VAWT concept for improved power generation," *Proceedings of Wind2003, 2003 ASME Wind Energy Symposium*, January 6-9, 2003, Reno, Nevada, USA.

Vandenberghe, D, and Dick, EA (1986), "Theoretical and experimental investigation into the straight bladed VAWT with second order harmonic pitch control," *Wind Engineering*, 10(3):122-138.

Viola, IM, Bot, P, Riotte, M (2013) "On the uncertainty of CFD in sail aerodynamics," *Int. J. Numer. Methods Fluids*, 72:1146–1164.